~~TOP SECRET~~/

BIF003W/2-180536-80 81

15 January 1981
Sheet Count: 31
Copy No.: 48

FARRAH PERFORMANCE AGAINST MODERN THREAT SIGNALS

VOL I

CLASSIFIED BY: BYE-1
REVIEW ON 1/15/2001

HANDLE VIA BYEMAN CONTROL SYSTEM ONLY

~~TOP SECRET~~

FOREWORD

This report is in three separate books:

Volume I	FARRAH Performance Against Modern Threat Signals – BIF003W/2-180536-80, dated 15 January 1981
Appendix A	Probability of Signal Detection – BIF003W/2-180536-80, dated 15 January 1981
Appendix B	Exemplary Emitter Parameters – BIF003/2-5617-80, dated 15 January 1981

CONTENTS

Section Page

SYMBOLS AND ACRONYMS

A/B	Monopulse antenna pattern amplitude ratio
AI	Airborne intercept (radar type)
B, BW	Antenna 3-dB beamwidth or bandwidth
BN	Beacon (signal type)
B_N	Noise Bandwidth
Bp	Predetection filter bandwidth
BS	Battlefield surveillance (radar type)
Bv	Low pass video filter one sided noise bandwidth
C	Angular noise model threshold sensitivity scale factors
C/D	Monopulse antenna pattern amplitude ratio
CW	Continuous wave (signal type)
D	Parabolic antenna diameter
dB	deciBels (power ratio)
dBm	Power ratio to 1 milliwatt in dB
DF	Direction finding (angle of arrival determination)
DT	Data transmission (signal type)
E	Elevation angle from a target signal to the spacecraft
E_N	rms power caused by thermal noise
E_{S+N}	rms power when both a signal and noise are present
ERP	Effective radiated power
EW	Early warning (radar type)
f	frequency
FAR	False alarm rate due to thermal noise
f(t)	Function of time
ft	Feet
GCI	Ground controlled intercept (signal type)
GHz	Gigahertz (radio frequency in billions of Hertz)
GSS	General System Specification

h	Height (satellite average altitude)
IF	Intermediate frequency (receiver section)
IM	Target illuminator (radar type)
K	Monopulse gain slope
km	Kilometers (thousands of meters)
kpps	Thousands of pulses per second
LD/SD	Look down/shoot down
LP	Long pulse (format descriptor)
MG	Missile guidance (radar type)
MHz	Megahertz (radio frequency in millions of Hertz)
n	Counting Index
N	Number (of pulses intercepted)
NF	Noise figure (of a receiver)
nmi	Nautical miles
P	Probability or pulsed (signal type)
PD	Pulse doppler (radar signal type)
P_D	Probability of signal detection
PRF	Pulse repetition frequency
PRI	Pulse repetition interval (inverse of PRF for constant pulse rate)
PSK	Phase shift key (signal coding type)
PU	Pulsed (signal type)
R	Slant range (from intercept signal to spacecraft)
RC	Resistor-capacitor (circuit type)
r_e	Radius of the earth
RF	Radio frequency
rms	Root mean square
SLERP	Sidelobe effective radiated power (usually taken to be 10 dB below transmitter power)
SNR	Signal to noise (power) ratio
SPO	System program office
t	time
TA	Target acquisition (radar type)
TCF	Transition current FARRAH
TCFM	Transition current FARRAH modified

TI	Technical Intelligence (analog receiving and recording system)
TIF	Transition improved FARRAH
[redacted]	
TT	Target track (radar type)
$\beta\tau$	Bandwidth times pulse width
Δ	Symbol for monopulse antenna difference pattern
λ	Wavelength (speed of light divided by signal RF)
μSEC	microseconds
Σ	Symbol for monopulse antenna sum pattern
σ_n	Thermal noise variance (statistical descriptor)
θ	Earth central angle (from emitter to subsatellite point)
ω	Angular rate in radians/second (filter pole)

Section 1
INTRODUCTION AND SUMMARY

A task was performed during the 1980 Advanced Low Orbit Elint Collection System Study to assess potential performance against modern threat signals for two configurations that had been developed during the study. The first configuration is called Transition Current Farrah (TCF) and uses an unmodified Farrah payload in a Shuttle-compatible spacecraft structure. The second configuration is called Transition Improved Farrah (TIF) and was designed to provide significant improvements in performance. A comparison of these two configurations against a specific set of exemplary signals (Appendix B) initiated a second task which was to investigate modifications to TCF that would improve its performance without requiring the development of TIF. This third configuration was called Transition Current Farrah – Modified (TCFM). It is currently planned to incorporate the TCFM sensitivity improvements in the Farrah III baseline.

This report is a summary of the computational methodology and the resultant threshold sensitivity and geolocation performance of the FARRAH Shuttle transition configurdtion (TCF), of an improved FARRAH configuration (TIF), and of FARRAH modifications to improve the intercept sensitivity for modern threat signals (TCFM). Previously presented material is summarized with emphasis on the modern threat signal intercept performance. In separate volumes, Appendix A provides additional theory and details of the threshold sensitivity computations and Appendix B provides paramters of the modern threat signals which were studied.

The performance of the three configurations against certain exemplary signals is summarized in Fig. 1-1. Those weapon systems and emitters listed along the left side of the figure comprise high interest Soviet emitters (see Appendix B), and are expected to be widely deployed in the late 1980s. The emitters are representative of newer technology radars. The second column indicates the function of the

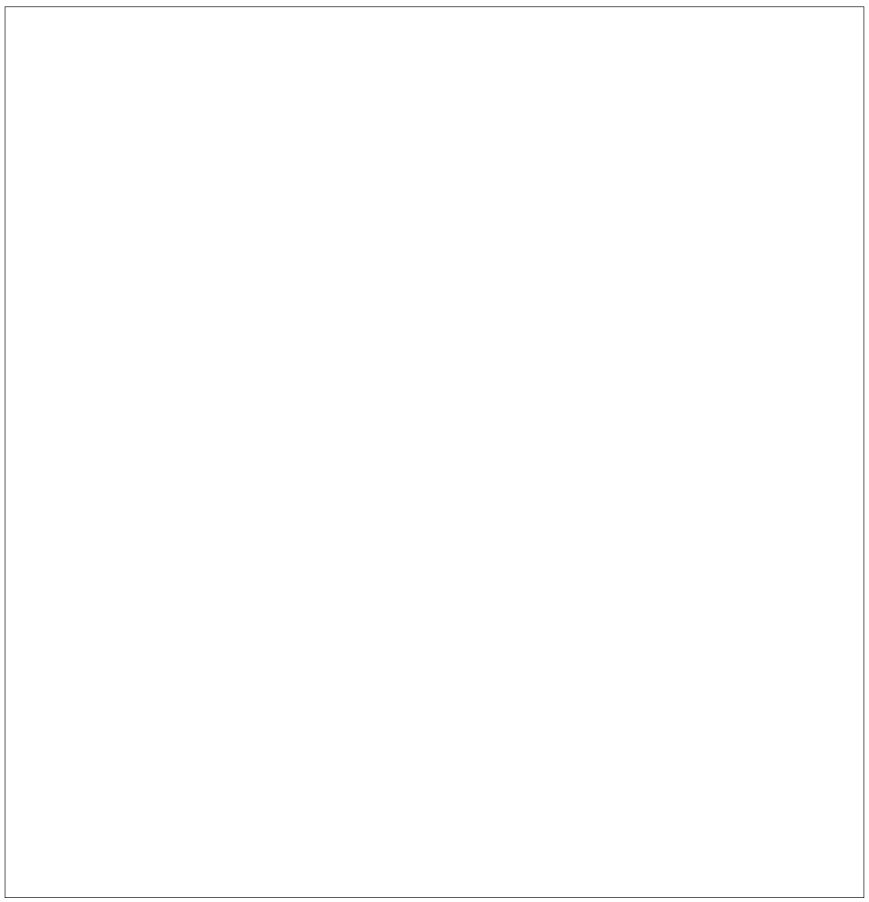

Fig. 1-1 FARRAH Performance Against Modern Threat Radars

emitter (e.g., EW means Early Warning Radar) and its characteristics. The next three major columns indicate the performance of the three configurations against each signal. The slant ranges used for the chart are 600 nmi for TCF and TCFM, 800 nmi for TIF. Within each major column are three subcolumns. These indicate, respectively, the probability of detection, geolocation accuracy in terms of the radius in kilometers of the equivalent 95 percent circular error probability circle, and the receiver in which the signal is intercepted. For example, the second line shows performance against the TCF intercepts its mean sidelobe ERP with probability 1, but must use the CW receiver to do so. TCFM and TIF intercept it using their pulse receiver (note that the TCF CW receiver intercept does not yield pulse characteristics). The geolocation accuracy for TCF is for TCFM and for TIF. These results and the additional results in Section 3 show that

the increased performance of TCFM (FARRAH III) relative to TCF provides a major improvement in modern threat signal performance at moderate cost.

Section 2

DESCRIPTION OF CONFIGURATIONS

The configurations as currently defined are the Shuttle transition version of current FARRAH (TCF), a modified version to improve sensitivity for intercepting new high interest signals (TCFM), and a Transition improved version (TIF). With the addition of a polarimeter, TCFM is identical with the currently defined baseline FARRAH III configuration. Familiarity with FARRAH I, which serves as a basis for comparison with the modified and improved versions, is assumed. Discussion is limited to the payload signal detection, parameter reporting, and geolocation performance.

Some of the more important characteristics of the three configurations are given in Fig. 2-1. Note that besides significant sensitivity differences, there are differences in collection time per day, frequency range covered, and assumed altitude.

Figures 2-2, 2-3, and 2-4 are block diagrams of the three configurations.

KEY FEATURES	TRANSITION CURRENT FARRAH
FREQ COVERAGE	2-18 GHz
DAILY COLLECT	6 HOURS
ORBIT ALT/INC	382 nmi
SENSITIVITY*	
– PULSE	76.5 dBm (0.1μS)/ 74.9 dBm (1μS)
– CW	56.5 dBm (100 kHz)

*ERP OF EMITTER; AT 10 GHz; SLANT RANGE 600 nmi FOR TCF/TCFM, 800 nmi FOR TIF; PROBABILITY OF DETECTION = 0.95

Fig. 2-1 Transition System Alternatives

2.1 TCF CONFIGURATION

TCF is essentially FARRAH-I as repackaged for launch by either the Shuttle or an unmanned booster. The system has three pencil beam antennas 120 spin degrees apart with dual mode cavity backed four-arm flat spiral feeds wired to produce a sum and a difference pattern. The reflector diameters are 6 ft from 2 to 6 GHz, 3 ft from 6 to 12 GHz, and 3 ft from 12 to 18 GHz. The payload has a 2 to 4 GHz IF passband into which a different 2 GHz RF band is switched each one-third spin. The sum and difference patterns are added with multiples of 90 deg phase shifts in the IF passband to produce amplitude comparison monopulse A, B, C, and D beams. There are dual omni antennas in each band for main beam intercept and, with a guard antenna, to provide sidelobe inhibit for the pencil beam antennas. Each 2 GHz payload channel has a square law detector and a nominal 7.5 MHz single pole video low pass filter.

The conditions for TCF pencil beam antenna pulse digitization are that the pulse be above a fixed detection threshold in the antenna sum channel and stronger than in the sidelobe inhibit patterns by a commandable inhibit margin. Detection is at the output of a 7.5 MHz video filter following each 2 GHz predetection filter and detector. The digitized parameters are the sum channel amplitude and threshold crossing time (TOA), the A/B, C/D, and sum/difference monopulse ratios, PW, and RF. For the PW measurement, the pulse must exceed the sum channel threshold by 4 dB. PW is then measured as the time from the pulse leading edge threshold crossing to the time at which the pulse drops to 3 dB below the peak measured value. Radio frequency (RF) is measured by the Pulse Frequency Measurement device (PFM) at the output of a bank of 64 filters with 3 dB crossover bandwidths of 31.25 MHz. There are three fast tuned 50 MHz pre-D filters with discriminators which are set on the (up to) three highest amplitude above-threshold filter outputs to obtain fine RF on up to three frequencies of a multiple RF signal.

The TCF CW subsystem uses a pair (direct and image) of 8 MHz multipole filters centered 60 MHz to either side of an LO which is swept in a linear sawtooth motion back and forth across the 2 GHz IF passband at a rate of 4/3 MHz per microsecond.

The resultant output of the 8 MHz filters is a pair of 6 μsec pulses with 8 MHz chirp in opposite directions spaced 90 μsec apart with a PRF repeat interval of about 3.3 msec (300 pps) and an average PRF of 600 pps. The direct and image swept filter channels are separately processed through square law detectors and 0.125 MHz single pole video low pass filters. Each sweep must produce a direct and image response which exceed both threshold and the inhibit margin to be digitized as a pencil beam CW intercept. There is a further commandable criterion that the detected PW must exceed 4 μsec as an additional guard against pulse digitization by the CW subsystem. The measured CW parameters are the monopulse parameters, signal amplitude, and time of arrival (from which RF is derived).

Except for the monopulse features, the omni antenna receivers and measured parameters are the same as for the pencil beam intercept. An amplitude comparison is made to pick the strongest of the two omni pattern intercepts for parameter digitization. The omni RF settings can be commanded independently of the pencil beam settings.

The TI receiver includes a multimode superheterodyne receiver, a 0.75 MHz pre-D recording capability, and a bandwidth compression capability which allows the recording of a short sample of wideband (10 MHz) predetected data.

2.2 TCFM CONFIGURATION

[redacted]

[redacted]

2.3 TIF CONFIGURATION

[redacted]

Section 3

SYSTEM PERFORMANCE

System performance is usually defined, for an ELINT collection system, in terms of its sensitivity, emitter geolocation accuracy, and its ability to identify and/or characterize the signal intercepted. In the FARRAH system, signal identification is normally accomplished by analysis of the digitized pulse or CW parameters collected. Characterization is accomplished by use of the TI receiver which takes handovers from the other receiver systems, and provides a sample of the predetected information for later analysis.

The system performance valuation has been concentrated on the DF system sensitivity and geolocation accuracy, and the main beam system (omni intercept system) sensitivity.

System sensitivity is computed in terms of the minimum effective radiated power (ERP of an emitter) that can be detected at a given slant range. A discussion of the equations and system parameters used for the various configurations is given in Section 4.

[redacted]

3.1 DF SYSTEM-MODERN THREAT SIGNAL PERFORMANCE

The results presented in this section are those generated by the current computer program and previously presented in briefings.

3.1.1 Analysis Method

To provide an unambiguous comparison between TCF, TCFM, and TIF, their performance is compared against a set of exemplary modern threat signals provided by the Program Office (Appendix B). These represent samples of current emitters of high mission interest and are considered representative of the types of signals to be encountered increasingly during the operational life of the system.

A basic mission objective of the system is to provide a high probability of intercept over the full RF band of interest and a wide geographic area on each pass over areas of interest. To compare the different configurations in an easily visualized manner, the swath widths corresponding to a specified probability of detection have been computed for each exemplary signal. The swath width is defined (for the purpose of this report) as twice the ground range from the subsatellite point to the emitter. Thus, the basis of comparison is related to the area over which each configuration can achieve a specification probability of detection.

3.1.2 Assumptions and Ground Rules

The basic assumptions and ground rules are summarized in this section and there is a brief discussion of the computer model used to obtain the results.

Performance has been analyzed for probabilities of detection of 0.5 and 0.95 for comparison purposes. These probabilities are for a single pulse or, for CW signals, a single receiver scan. Since the instantaneous bandwidths are not the same (2 GHz for TCF [redacted]), the false alarm rate (FAR) is set at 1 sec/GHz for analysis. For these probabilities of detection and the selected FAR, the SNR required in the pre-D bandwidth is determined as a function of PW for each configuration. (See Appendix A.)

Sidelobe ERPs for the emitters have been set at 10 dB below isotropic (mean sidelobe ERP) in almost all cases (see Appendix B for ERPs used).

A polarization loss of 3 dB is assumed and the DF antenna pointing loss used is 3 dB. This is a conservative assumption, but one which permits intersystem comparison.

The TCF antenna gains and losses are taken from 1979 CDR data. For TCFM and TIF, they are taken from 1980 calibration data. The differences are not large, but will be reevaluated as more data on FARRAH I becomes available.

For TCFM and TIF, the noise figures are from an analysis of manufacturers data and cable and beam forming network losses are by analysis from standard available data. Propagation losses are computed from a standard model.

The computer analysis incorporates a master program, an emitter file, and files for each configuration. The emitter file contains, for each emitter, an identifier, the frequency, a flag for CW, a flag for pulse doppler signals, the PW, PRF, and ERP. The pulse doppler flag is used to address a special loss factor for pulse signals in the CW receivers.

The configuration files contain altitude, antenna, and cable losses as a function of frequency, pre-D SNR required for $P_D = 0.5$ and $P_D = 0.95$ as a function of pulse width, noise figure as a function of frequency, and pre-D bandwidths.

For each emitter the program starts with a reference slant range of 600 nmi for TCF [redacted] and computes the range and propagation losses as a function of frequency and elevation angle of the vehicle. The antenna and other losses are then computed and the system temperature computed from the antenna temperature and noise figure. Putting in the fixed pointing and polarization loss and the nominal gains the pre-D SNR is computed and compared with the pre-D SNR required as a function of PW for each configuration. The slant range required to just meet the required SNR is estimated by an inverse square calculation and the entire loop iterated until the slang range just meets the required SNR, or becomes

less than the altitude, or behond the horizon. Then the cross range and swath width are computed and output. There are a few additional refinements. The antenna temperature, for example, is computed as a function of the fraction of the main beam off the earth and sky temperature as a function of frequency.

Geolocation data for several values of the semi-major axis are also computed. (For details of the accuracy analysis, see Section 5.)

As a feature of the program, if a pulse doppler signal is detectable in the pulse receiver, CW intercept of that signal is not analyzed. Out of RF band emitters for TCF/TCFM are also noted.

3.1.3 DF System Performance Results

The results of the performance analysis made on the exemplary signals described in Appendix B are summarized in Fig. 3-1, 3-2, and 3-3.

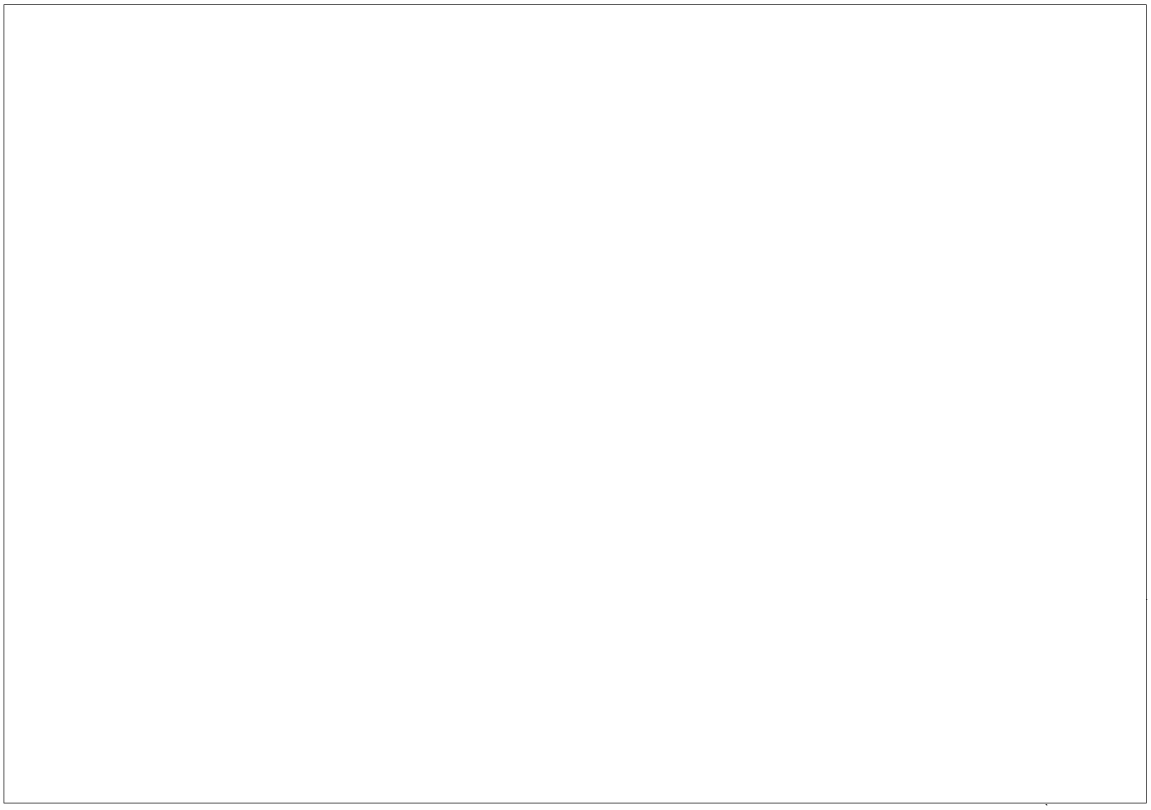

Fig. 3-1 FARRAH Collection System Performance Modern Threat Radars

The weapon systems and emitters listed along the left hand side of Fig. 3-1 comprise high interest Soviet emitters, which are expected to be in moderate to heavy use in the late 1980s. The second column indicates the type of emitter and its characteristics. The two performance measures indicated in the figure are the swath width for a given detection probability and swath width for a given geolocation accuracy. For example,

The bar graph shows that TCF will intercept the median sidelobes of this signal over a swath width of 1940 nmi with a probability of 0.95 or greater. It will intercept it with a probability equal to or greater than 0.5 over a swath width of 2350 nmi. The swath width over which geolocation accuracy is or better is 1160 nmi. For accuracy the swath widths are 800 and 520 nmi, respectively.

The first set of 10 signals clearly shows the difference between the three configurations.

Detection performance against additional modern emitters and a repeat of the pattern is shown in Fig. 3-2 and 3-3.

3.2 MAIN BEAM INTERCEPT PERFORMANCE

The FARRAH omni receiver subsystems have the same basic sensitivity as their pencil beam counterparts (disregarding antenna gain difference). However, the omni antenna patterns cover more space than earth resulting in a lower antenna temperature than for the pencil beam system.

3.2.1 Overview

The sensitivity of the various configurations has been analyzed for main beam intercept by the omni antennas. The intercept receiver noise figures and cable losses were evaluated using the same basic configurations as the DF system. The key problem is the analysis is to establish a usable model for the omni gains and temperatures.

3.2.2 Omni Antenna Orientation

At any given point around the orbit, the axes of the omni antennas are oriented differently with respect to the earth than at any other point. Thus the gain distribution varies with respect to the subsatellite point and, because the antenna temperature is primarily driven by the portion of the pattern intercepted by the earth, the temperature varies around the orbit.

For the lower bands, the omnis have the poorest performance when the antenna axis is pointed at nadir, because the gain near the horizon is well down and the temperature is a maximum. For the high band biconical antenna, the worst case is with the axis normal to the radius vector, a horizontal orientation. These cases were assumed for analysis. Because in this orientation, the biconical has a gain variation in azimuth, a 45 deg angle was selected as representative. This 45 deg assumption is more conservative than taking the average gain over all azimuths.

3.2.3 Patterns

The lower band omnis were taken to have a cardiodal pattern in voltage. This was checked against the calibration data and fit well through the central portion down to about the 6 dB points.

The upper band biconical was given a simple toroidal pattern with a cosine cross section in the E field. Again, this agrees fairly well with the calibration data. The on-axis gains vs frequency were then taken from the measured values of the Current FARRAH omnis. The relative gains are then taken from the cardiodal and cosine patterns. The omni temperatures were computed numerically. The results are:

OMNI TEMPERATURES

ALTITUDE (nmi)	CARDIODAL PATTERN	TOROIDAL PATTERN
382	213 K	80.6 K
600	190 K	74.5 K

3.2.4 Performance Against Exemplary Signals

The gains, noise figures, antenna temperatures, and losses were entered in a computer program and the detection performance established against the same exemplary signals used for the DF system (described in Appendix B). Emitter pointing losses of 3 dB were assumed except for essentially omni beacon emitters where 1.5 dB was assumed. The results are summarized in Fig. 3-5, 3-6, and 3-7. For each emitter the swath width (twice the cross range from the subsatellite point) is shown for 50 percent and 95 percent probability of detection. For reference, the elevation angle of the satellite (from the emitter) at the detection limits is given in degrees. These results are discussed in Section 3.3.

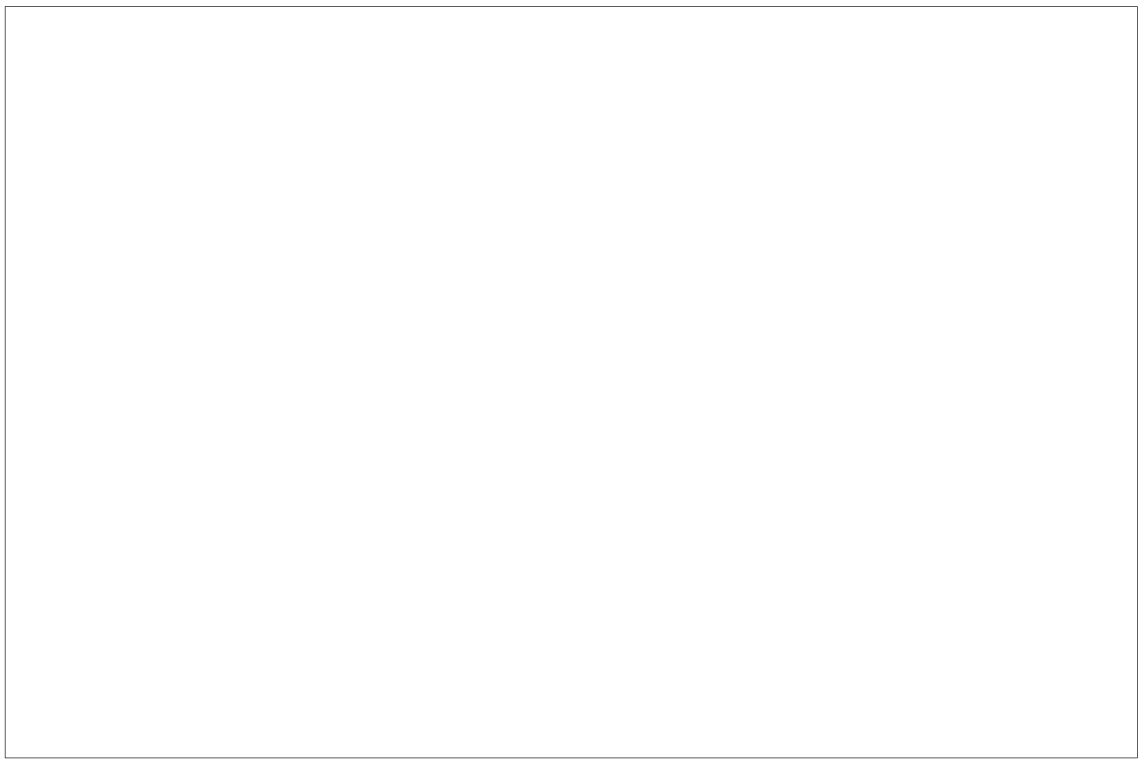

Fig. 3-7 FARRAH Main Beam System Performance Against Supplementary Representative Signals

3.3 RELATIVE CONFIGURATION PERFORMANCE

The modern threat signal collection performance of the three configurations, TCF, TCFM, and TIF, has been shown in Fig. 3-1, 3-2, and 3-3 for sidelobe intercept and in Fig. 3-5, 3-6, and 3-7 for main beam intercept. The primary deficiency indicated in Fig. 3-5, is that TCF has signals. Given the generally low probability (1) of main beam intercept of these radar types, (2) that main beam intercepts tend to be concentrated near the horizon, and (3) that the best opportunity for the TI receiver to observe mode changes and signal formats is during main beam intercepts,

For the supplementary representative signals of interest, an inadequate main beam intercept sensitivity of all three configurations is shown in Fig. 3-5 for the

For pencil beam intercept (DF system) of the modern threat signals, both intercept sensitivity and location accuracy are important. Relative modern threat signal pencil beam performance of TCF, TCFM, and TIF is shown in Fig. 3-1. TCF has marginal intercept sensitivity for nearly all of these signals.

TCF has inadequate nadir pulse subsystem sensitivity for the radar pulsed signals but can intercept them in the CW subsystem at a reduced probability of intercept as indicated in Fig. 3-1. This is an undesirable operational mode in that additional information is needed to distinguish the resultant intercepts from CW signals.

[redacted]

Section 4

SENSITIVITY CALCULATIONS

Sensitivity calculations involve two fundamental and separable portions; (a) link performance and (b) receiver threshold detection performance. Link performance is a function of emitter ERP, slant range, propagation losses, antenna gain, and system noise figure. Threshold detection performance is a strong function of the receiver configuration, especially the ratio of predetection to post detection bandwidths.

Link performance is discussed in Section 4.1. Threshold detection sensitivity is covered briefly in Secton 4.2, and in greater detail in Appendix A.

4.1 INTERCEPT LINK PERFORMANCE

A sample calculation is given in Table 4-1, to indicate the methodology. It is done for a pencil beam (DF system) intercept at $P_D = 0.5$ of a 0.1 μsec pulse at 10 GHz, at a slant range of 600 nmi. Note that this sample calculation does not include propagation (atmospheric absorption) loss which is computed from a standard model and is entered into each actual link calculation by the computer. Also, not shown here is the computation of antenna temperature which first determines the portion of the intercept antenna beam that intersects the earth, vs that which intersects the sky.

The path loss term in the above computation is given by

$$\text{Path Loss} = 20 \log (4\pi R/\lambda) = 20 \log \left[\frac{f\,(\text{MHz})}{1000} \frac{R\,(\text{nmi})}{1000}\right] + 157.8 \text{ dB}$$

Table 4-1
SAMPLE LINK CALCULATION

Parameter	TCF
P_D = 0.5 SNR (from Fig. 3-2) (dB)	19.7
Thermal Noise in 10 MHz (dBm)	-103.9
Required Signal Power (dBm)	-84.2
10 GHz Antenna Gain (dB)	31.7
Polarization and Pointing Loss (dB)	-6.0
Receiver Noise Figure (dB)	-10.1
600 nmi 10 GHz Path Loss (dB)	-173.4
Net Transmission Loss (dB)	-157.8
Required Signal Power (dBm)	73.8

[redacted]

Antenna gains are a function of frequency and configuration. Data on these gains are shown in Fig. 4-1. The TCF data is from the April 1979 P-989 CDR.

[redacted]

Noise figure data shown in Fig. 4-1 is based on 1979 CDR data for TCF, and on analysis of vendor survey data for TIF and TCFM

4.2 THRESHOLD DETECTION SENSITIVITY

Threshold detection sensitivity is a strong function of the absolute value of the predetection and video bandwidths, and their ratio. It is important to know filter characteristics so that noise bandwidth and pulse response can be characterized.

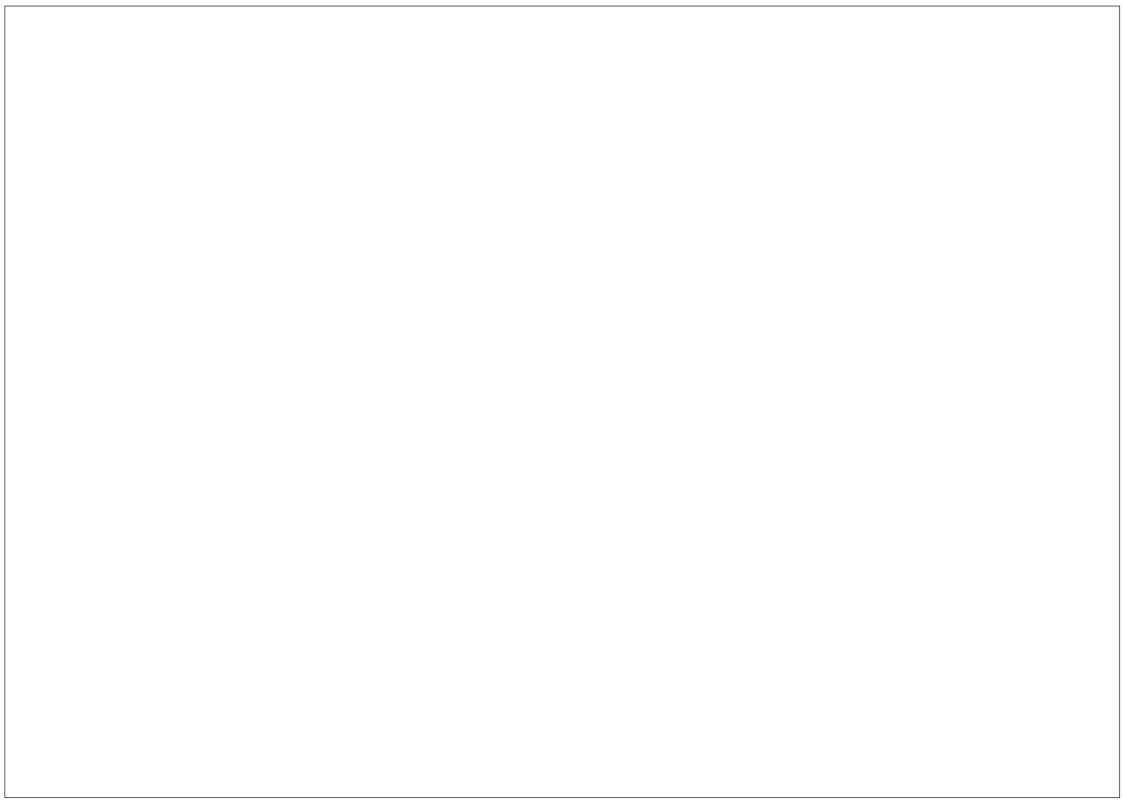

Fig. 4-1 Pencil Beam Antenna Gains and Noise Figures

The FARRAH threshold detection sensitivity estimates herein have been derived from a combination of theoretical and measured results. The video filters are approximately single pole but are nonlinear and have not yet been accurately characterized. [redacted]

[redacted]

4.2.1 Mathematical Models

Appendix A contains a detailed discussion of the following mathematical models.

For the TCF wideband crystal video receiver implementation, the video noise with or without a pulse present has a Gaussian distribution. The video detection threshold is set for a false alarm rate (FAR) of once per second with no input signal. The time between crossings of the mean by Gaussian noise has an exponential distribution. The threshold setting for a specified FAR can be derived as

$$SNR = 2 \ell n \; B_V / \sqrt{3} \; FAR \qquad (1)$$

where B_V is the video low pass filter noise bandwidth.

For a crystal video system with square law detection, the pre-D signal-to-noise ratio (SNR_P) required to reach threshold is obtained as the ratio of video energy with a signal present to the noise only case. This relationship is

$$SNR_T = \frac{E_{S+N}}{E_N} = \frac{1}{(1 - B_V/2B_P)} \left[SNR_P^2 \; (B_P/2B_V) + 2 \; SNR_P + (1 - B_V/2B_P) \right]$$

where the SNRs are expressed as numerics rather than dB.

Solving this for the pre-D SNR

$$SNR_P = \frac{2B_V}{B_P} \left\{ -1 + \left[1 + \left(\frac{B_P}{2 \, B_V} - 0.25 \right) (SNR_T - 1) \right]^{1/2} \right\} \qquad (2)$$

where B_P is the pre-D filter bandwidth.

The above formulation applies to the 50 percent probability of detection (P_D) of pulses approximately matched to the video filter response bandwidth ($PW = 0.5/B_V$) and assumes that the video pulse reaches full amplitude without overshoot. For a single pole low pass filter, the unit step response is

$$f(t) = 1 - e^{-\omega t}, \qquad \omega = 2\pi \frac{2}{\pi} B_V, \qquad \text{matched } \omega t = 2 \tag{3}$$

the peak amplitude response to a unit pulse of width $0.5/B_V$ is thus 0.865 (down 1.26 dB). This 1.26 dB video filter response penalty must be added to SNR_T in deriving SNR_P.

For $P_D = 0.95$, the video pulse amplitude must be far enough above threshold to offset pulse riding noise at the 5 percent low end of the Gaussian distribution (subtracting from the pulse amplitude). This is at the 1.645 sigma (voltage) point on the distribution. The required SNR for $P_D = 0.95$ is obtained by replacing SNR_T in the above equation by

$$SNR_{0.95} = \left[\sqrt{SNR_T} + 1.645\right]^2$$

For PWs other than $0.5/B_V$, the filter response penalty can be computed as above. For longer pulses, the pulse riding noise has additional opportunities to cause a threshold crossing. The result is a lower pulse amplitude for a given P_D. If we define N as the number of independent noise pulse responses riding a long pulse (PW divided by $0.5/B_V$), the point, P, on the cumulative noise distribution is given by

$$P_D = 1 - P^N \text{ or } P = (1 - P_D)^{1/N}$$

Using P_D and the resultant value of P, enter a Gaussian cumulative distribution table to find the sigma increase from P_D to P. This is the voltage increment for pulse riding Gaussian noise and permits the pulse voltage to be lower by this

amount for the specified value of P_D. If the video filter has either overshoot or undershoot for the PW of concern then this must also be applied to the detected signal and noise pulses.

The FARRAH CW subsystem pre-D to video filter bandwidth ratio of 64/1 falls in a transition region between the theoretical performance of a crystal video receiver and a matched filter, defined as $B_P = 2\,B_V$, where $B_V = 0.5/PW$. For the matched filter the video noise with no signal has a Rayleigh distribution. The $P_D = 0.5$ detection threshold is then

$$SNR_T^* = \ell n \left[B_P/FAR\right] \qquad (4)$$

This is also the pre-D threshold SNR and is nearly 3 dB lower than the Eq. (1) crystal video filter threshold.

When a signal is present, the noise distribution tends to change from pure Rayleigh to Rician and, as the signal increases, it approaches Gaussian. Also, at the output of the low pass filter the signal assumes its peak value rather than its rms value. This is equivalent to reducing the noise by $\sqrt{2}$ (3 dB). Thus.

$$SNR^*_{0.95} = \left[\sqrt{SNR_T^*} + 1.645/\sqrt{2}\right]^2$$

The long pulse SNR reduction for noise spikes is computed as before but with the voltage increments computed as the Gaussian sigma changes divided by the square root of 2.

In a 1973 study, BIF-476W measured the $P_D = 0.5$ detection performance at a FAR of one per second of a 1 MHz two-pole Butterworth low pass video filter with 0.5 μsec input pulses as the pre-D bandwidth was varied from 3.2 MHz to 5 GHz. These measured points are compared to the computed performance in Fig. 4-2. The computed crystal video SNR Eq. (3) is also shown. For the

*SNR_T^* is used to differentiate matched filter case from crystal video case.

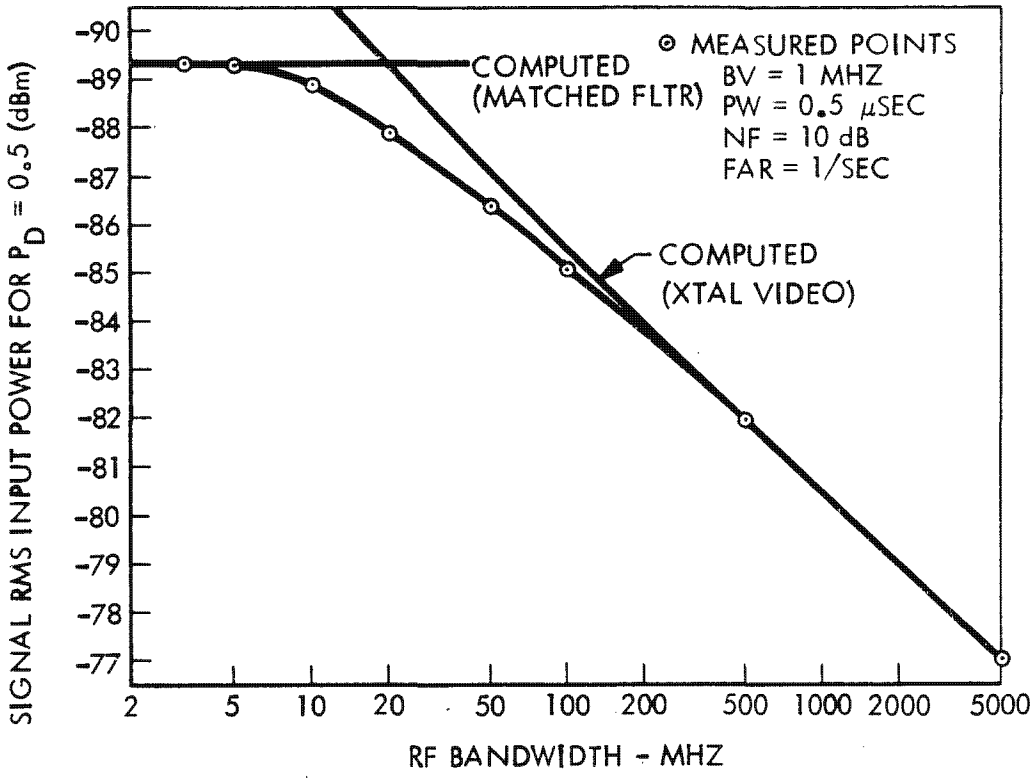

Fig. 4-2 Pulse RMS Input Power Required for P_D = 0.5

matched filter case, B_P = 2 MHz. The corresponding asymptote on Fig. 3-1 was computed as follows:

$$\text{Input Power} = 10 \log (\ell n\ B_P) + 10 \log KT\ B_P + 10 = -89.23 \text{ dBm}$$

where K is Boltzmann"s constant, T was nominally 300°K (80.4°F), and the stated receiver noise figure was 10 dB.

It is indicated in Fig. 4-2 that the matched filter computed performance is reliable for $B_P/B_V \leq 5$, the crystal video computation is reliable for $P_B/B_V \geq 200$, and that corrections are required at the intermediate bandwidth ratios. Note that Fig. 4-2 is a reliable correction curve only for conditions which result in the asymptotes of the two computations intersecting at a bandwidth ratio near 19/1.

For the transition region, performance can be approximated as a weighted average of the corrected performance as computed separately by the matched filter and crystal video formulations. For the FARRAH CW subsystem, for example, the indicated Fig. 4-2 discrepancy with the matched filter computation at the 64/1 bandwidth ratio is 3.5 dB and the discrepancy with the crystal video computation is 0.6 dB. The computed performance is then:

	Matched Filter	Crystal Video	dB Weighted
P_D = 0.5 Video Threshold (dB)	10.94	13.50	13.13
SNR in 8 MHz (dB)	-4.11	-1.06	–
Corrected SNR in 8 MHz	-0.01	+0.14	+0.12

The 2 GHz pre-D SNR is then +0.12 - 10 log (2000/8) or -23.86 dB. The corrected SNR is 8 MHz includes the above corrections plus 0.6 dB for the shaping of the 6 μsec pulse by the 8 MHz filter. The corrected values would be equal if the CW subsystem parameters resulted in asymptote intersection at the 19/1 bandwidth ratio of Fig. 4-2.

The unit step response of the two pole low pass Butterworth filter is

$$f(t) = 1 - \sqrt{2}^{-\omega t/\sqrt{2}} \sin(\omega t/\sqrt{2} + 45°) \qquad (5)$$

where, for a noise bandwidth B_V, $\omega = 5.66\ B_V$. This formula was used to compute the short pusle response and overshoot of the two pole TIF filters.

4.2.2 Comparative Configuration Performance

The past presentations of the sensitivity performance of future FARRAH configurations, and in Fig. 4-3 through 4-6, sensitivity has been referred to a 10 MHz pre-D bandwidth. This allows the direct comparison of various configurations when it is desired to show the effects of sensitivity improvements. Actual predetection SNR can be obtained by bandwidth ratioing. For example, if it is desired to change from this to a 2 GHz bandwidth, subtract 23 dB.

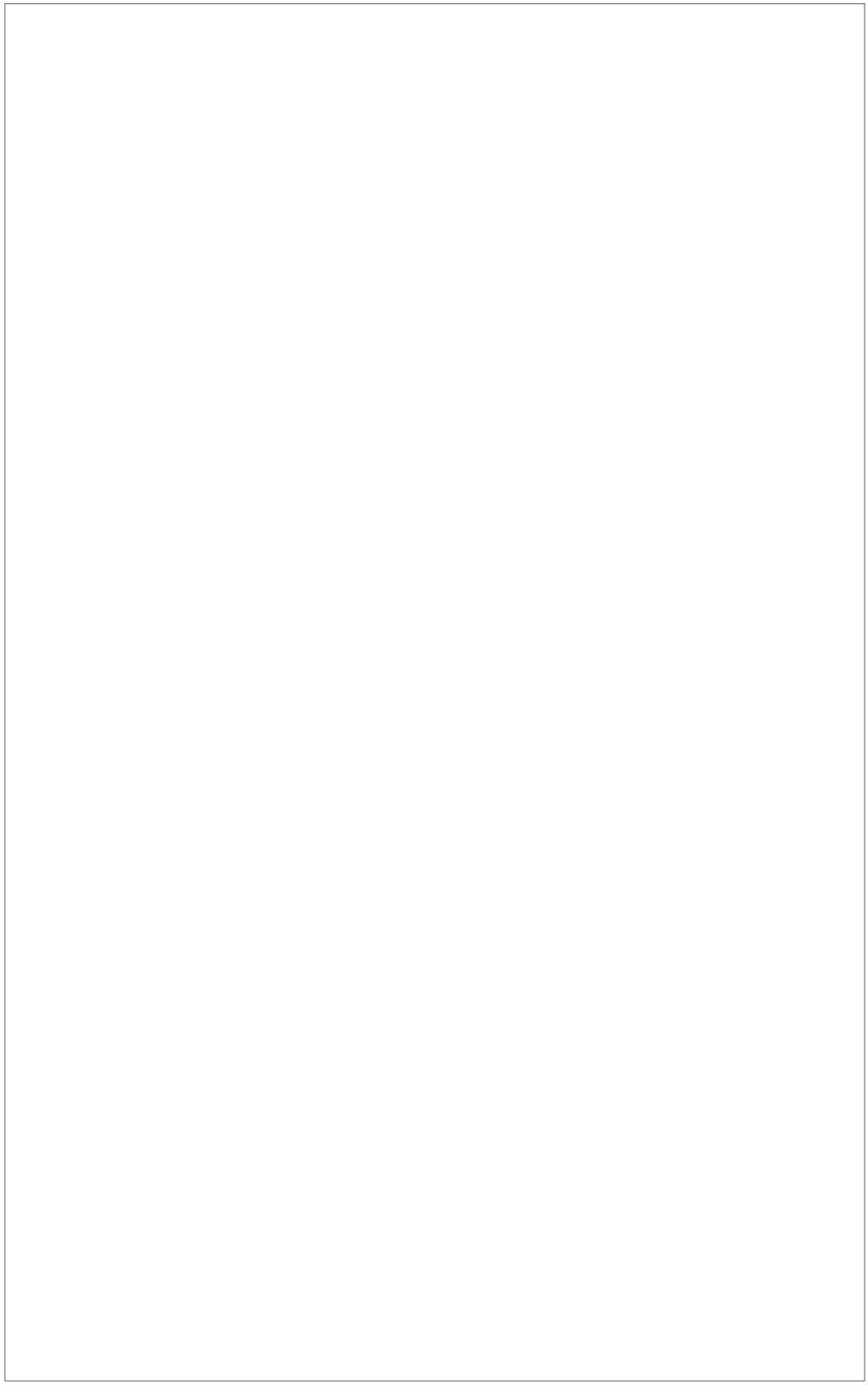

Fig. 4-4 FARRAH Pulse Collection Sensitivity at $P_D = 0.95$

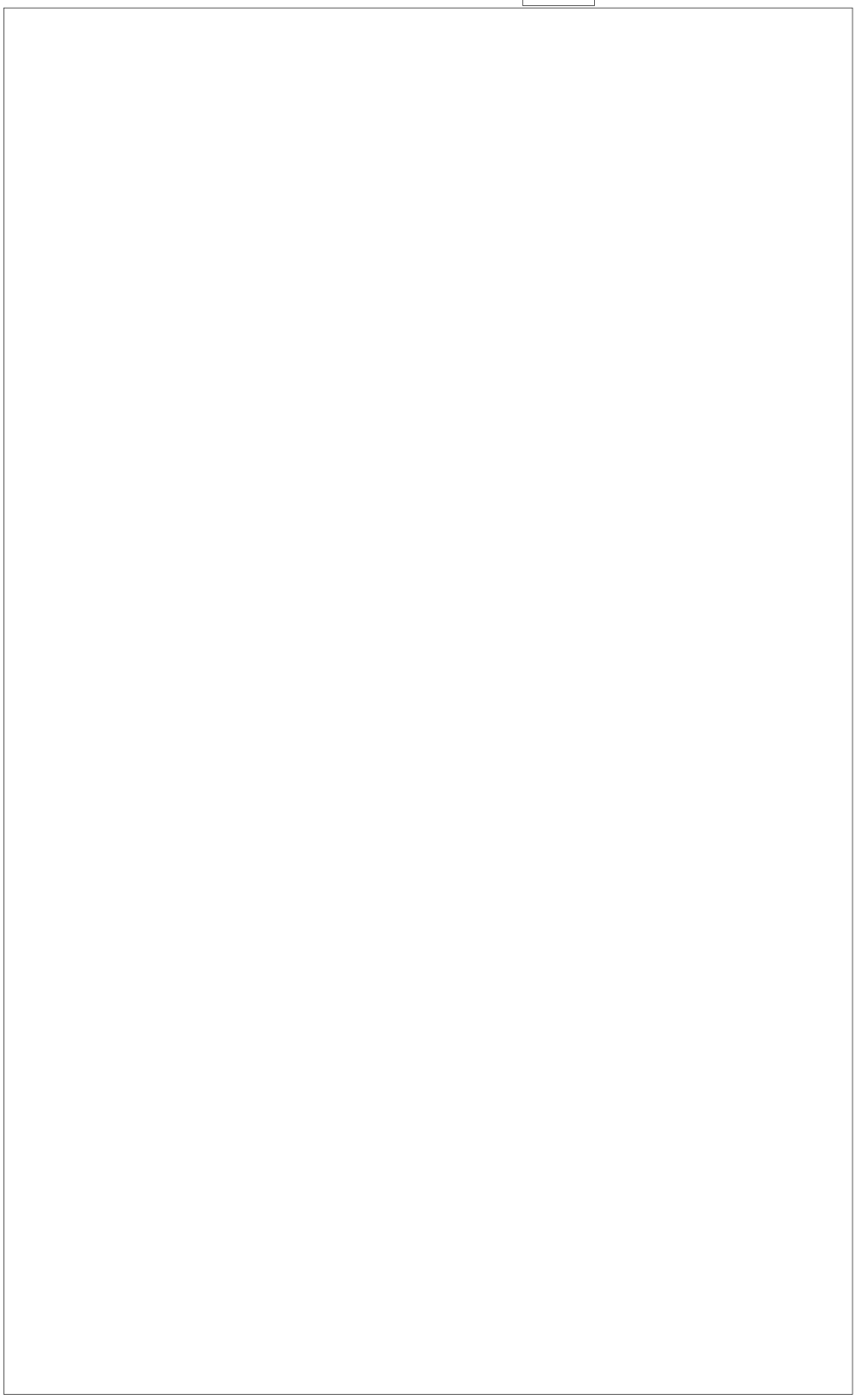

Fig. 4-6 FARRAH CW Subsystem Sensitivity for $P_D = 0.95$

The comparative $P_D = 0.5$ and $P_D = 0.95$ receiver sensitivities of TCF, TCFM, and TIF at a system FAR of 1 per second are shown in Fig. 4-3 and 4-4. The TCF long pulse sensitivity improvement is caused only by pulse riding noise rather than by a change in the post detection filter utilized. [redacted]

[redacted]

Because of the narrower bandwidth implementation, the FARRAH CW subsystem has about 20 dB more sensitivity than the pulse subsystem. The computed comparative CW subsystem performance is shown in Fig. 4-5 for $P_D = 0.5$ and Fig. 4-6 for $P_D = 0.95$. These are shown as a function of PW to illustrate the performance roll-off on the short pulses available from some of the pulse doppler signals. The sensitivity for CW intercept is the value at a pulse width of 6 μsec except for the

[redacted]

The current computations resulting in Fig. 4-3 through 4-6 represent additional refinement of the earlier computations used in the modern threat performance evaluation in that the detection theory has been more completely developed and the video filter performance better defined. The filter selection process is not yet finished and their parameters are expected to change during near future iterations.

The exemplary signal performance reported in Section 3 is not materially affected by these refinements, however, and has not been changed from earlier submissions.

4.3 MODERN THREAT SIGNAL CONSIDERATIONS

As a result of marginal sensitivity of the FARRAH pulse intercept system for certain modern threat pulse doppler signals of interest, and the 20 dB higher sensitivity of the CW subsystem, the conditions for CW intercept of pulsed signals has been evaluated. Because of the 90 μsec delay from the swept filter initial to confirming intercept, a pulsed emitter whose PRF is an integral multiple of 11 kpps will be intercepted by both 8 MHz filters if it is intercepted by either one. The probability of an 11 kpps emitter having the applicable pulse position phasing for CW intercept is (6 + PW)/90. The PW/PRF combinations for which pulses will overlap the TCF direct and image filters are shown in Fig. 4-7. For purposes of the plot, a CW signal is defined as one for which PW x PRF = 1. The transition curve between regions A and B is defined by PRI - PW = 6 μsec. The excluded regions are those within which no combination of partial pulse overlap with one CW filter also permits partial overlap with the other. The end of each spike is defined by the condition

$$PRF = \frac{n}{90 - 6 - PW} = \frac{n + 1}{90 + 6 + PW} \quad \text{or} \quad PW = \frac{84 - 12n}{2n + 1} \ \mu\text{sec}$$

where n is a positive integer.

Pulse overlap with each CW filter is a necessary condition for pulsed signal digitization by the CW subsystem but there is a sensitivity penalty for overlap of less than 6 μsec as illustrated in Fig. 4-5 and 4-6. Nonetheless, the TCF CW subsystem retains a sensitivity advantage of 7.3 dB for an overlap of 0.1 μsec compared to the pulse subsystem sensitivity. To achieve CW digitization of pulsed signals there is a PW $\geq$ 4 μsec logic check which must be disabled.

Because of the large sensitivity advantage of the CW subsystem, short pulses centered slightly outside the 8 MHz swept filter band will be intercepted. For example, a 0.1 μsec pulse has 10 MHz bandwidth and will appear with equal sensitivity in the pulsed and CW subsystems if it is centered approximately 3 MHz beyond the 8 MHz CW filter band edge.

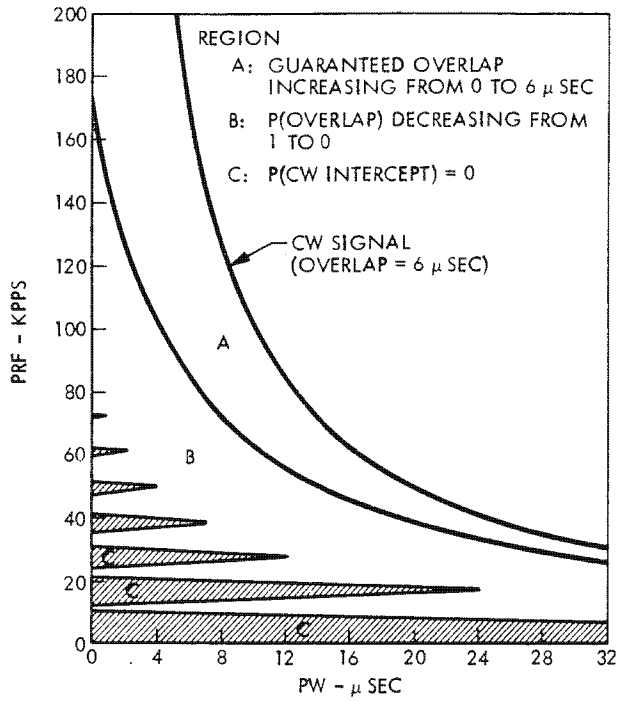

Fig. 4-7 Probability of CW Intercept of Pulsed Signals

The modern threat signals have many pulse format and coding modes which are not preserved in the FARRAH digital data. Because of this, TI receiver intercepts are highly desirable. These are accomplished by the signal recognition handover mode. The RF/PW/PRF ranges of interest are command stored in registers against which the digitized parameters are compared. When a within-range match occurs the TI receiver is set on the radio frequency and antenna of interest. This is either the pencil beam sum channel or the omni antenna in which the largest signal amplitude was measured. For CW subsystem intercepts, the only recognition parameter is RF. The TI receiver can center itself on the signal RF, perform a 10 MHz spectrum analysis and set the pre-D processing bandwidth to either 0.75 MHz or into the 10 MHz bandwidth compression mode. The latter mode will produce 250 μsec samples in FARRAH I.

URSALA-III, P-989 has almost zero drag orbits. Although the budget will probably be exceeded by more than 2/1, it is the current specification agreed to by the USAF Satellite Control Facility and is small enough to have negligible impact on geolocation performance. A 1000-ft ephemeris error results in a worst case angular error of only 0.025 deg at a 382 nmi slant range.

The past P-989 data processing terrain map had about a 1000-ft rms altitude error. For FARRAH, a new computerized Army mapping service terrain map quantized in 100 meter increments and with an estimated rms error of 300 ft will be used. From a 382 nmi orbit, the maximum angular error introduced by a 300-ft emitter altitude error is about 0.005 deg.

In the [redacted] computer simulation, the in-track ephemeris error is combined (RSS) with the semi-minor axis of the computed error ellipse, and the contributions of the emitter altitude error and the in-track and cross-track ephemeris errors are combined with the semi-major axis of the ellipse as computed from the other error sources. These errors are modeled as having a right circular conical distribution about the antenna boresight. The program computes the circular earth intercept triangle and elevation angle for the specified slant range or distance off nadir, and intersects the error cone with a tangent plane at the assumed emitter location to compute the error ellipse. The ellipse axial ratio (prior to including the ephemeris and emitter altitude errors) is thus the cosecant of the intercept elevation angle.

5.1.2 Platform Attitude Error

The assumed post calibration FARRAH attitude error is 0.045 deg (one sigma). It is estimated that this could be reduced to 0.02 deg through the use of star sensors (not currently planned). The FARRAH specifications contain a 95 percent angular error budget. In this study, the 95 percent budget is taken to be 2.45 times the one-sigma budget. The combined contribution of platform attitude, ephemeris, and emitter altitude error to the 95 percent budget is assumed to be 0.12 deg.

Section 5
GEOLOCATION PERFORMANCE

The predominant source of FARRAH geolocation inaccuracy is the residual electronic measurement error. This error results in a direction finding (DF) error proportional to antenna beamwidth. Its major components are antenna pattern errors as a result of the unknown incoming signal polarization, residual biases and model imperfections, and thermal noise error. The ability to improve the model and bias errors is ultimately limited by measurement uncertainties including the on-orbit component temperatures, fine grain antenna pattern ripple from a large number of sources, and the inability to separate multiple contributing sources.

Nonpayload dependent error sources are the ephemeris error, the emitter altitude uncertainty, and the residual vehicle attitude and sensor boresight uncertainties.

The FARRAH detection sensitivity and geolocation error models have been incorporated in a computer program and used to generate general and signal specific performance charts of which a set of bar charts for the modern threat signals is presented in Section 3.1.

5.1 CONFIGURATION INDEPENDENT ERRORS

The errors which are assumed to have the same levels for the various versions of FARRAH are the nonpayload dependent errors and the payload biases.

5.1.1 Ephemeris and Emitter Altitude Errors

Based on past P-989 ephemeris analysis, a one-sigma predict (data processing) ephemeris error of 1000 ft in-track by 200-ft cross-track by 200-ft altitude has been assumed. Past experience included high drag orbits whereas, starting with

In ground test, there is no satisfactory way to measure the spin axis to body coordinate angles to 0.045 deg accuracy. Instead, the spacecraft has two horizon sensors and three sun sensors whose alignments to the body are measured to about 0.01 deg accuracy. The sun sensors provide a direct measure of the free flight spin axis to body coordinate angles. The sun sensors provide an elevation angle quantized in 0.5 deg steps over a 64 deg range and a spin clocking pulse. With time, the sun elevation angle transitions between 0.5 deg quantization steps. These transitions and the clocking pulses provide an angular reference accuracy of about 0.02 deg and are the key to achieving on-orbit attitude reconstruction to 0.045 deg. Calibration pass analysis provides comparable accuracy in antenna electrical boresight attitude reconstruction. The combined 95 percent error could be reduced from about 0.12 deg to about 0.05 deg through the use of star sensors. The above errors have significant impact at the high end of the intercept RF range but are negligible compared to the payload error budget at 2 GHz.

5.1.3 Monopulse Gain Slope

The system electrical errors can be expressed as dB errors in terms of their impact on the monopulse angle of arrival accuracy. On average, an error of 1 dB in the monopulse ratios causes an angular error of 0.06 B where B is the antenna 3 dB beamwidth. In the current study the antenna beamwidth has consistently been computed as 70 λ/D (corresponding to ideal feed taper) whereas the measured beamwidths of the program antennas average about 64 λ/D (vs 57.3 λ/D for uniform aperture illumination).

5.1.4 Electrical Bias Errors

The error budget terms that are modeled as monopulse biases which remain constant from pulse-to-pulse are the polarization error and the channel mismatch error.

The polarization error results from the antenna pattern response to the unknown polarization of the incoming signal. Each antenna has a cavity backed four arm flat spiral feed to generate a sum (Σ) and difference (Δ) pattern. The Σ pattern

is in phase with the Δ pattern at a reference azimuth which rotates with frequency and has relative phase shifts equal to azimuth changes at a fixed frequency. The Σ and Δ patterns are added at RF with multiples of 90 deg relative phase shifts to generate the TCF monopulse A, B, C, and D beams. The planned TIF monopulse measurements are the Σ/Δ ratio (angle off axis) and the Σ/Δ phase difference (azimuth).

The DF antenna patterns are circularly polarized on axis going to highly elliptical at the beam edges. The variations in measured monopulse angle of arrival with a spinning linearly polarized source have an average rms value of 0.02 B which is the assumed polarization error. The error grows rapidly with angle off boresight, is negatively correlated on opposite sides of boresight, and causes boresight direction fluctuations for signals near boresight. Because the dominant system error source at high SNRs is the polarization error, improved modeling or measurement of received signal polarization might be worth while. At the cost of another set of hybrids to generate a LHCP sum channel pattern and another receiver and measurement channel, the received polarization of each pulse could be measured. With such a polarimeter, quantization of the LHCP to RHCP power ratio to 1/8 dB, of phase between the two patterns to 20 deg, and a polarization error look up table it is estimated that the residual polarization error could be reduced to 0.005 B (equivalent to 0.083 dB in pulse power). Measurement of pencil beam signal polarization is not currently planned because of cost.

A post calibration residual monopulse channel mismatch exists because of inexactly matched components and unknown temperature differences. The estimate of the rms channel mismatch over the frequency range at typical temperature mismatches is 0.17 dB which will produce a monopulse angular bias error of 0.01 B.

5.2 CONFIGURATION DEPENDENT ERRORS

The above errors are assumed to apply equally to the pulse and CW subsystem of TCF, TCFM, and TIF. Errors which are independent from measurement to measurement or which depend on signal level require implementation peculiar modeling,

5.2.1 Thermal Noise

FARRAH uses a beam forming network which forms four skewed beams; A, B, C, and D, plus sum and difference. The SNR of the ABCD beams will be different than the sum beam depending on the location of the target with respect to boresight. The monopulse error caused by thermal noise can be expressed as a function of the SNR of these beams.

The P-989 thermal noise monopulse power ratio error has been derived as

$$\sigma_{A/B} = 4.34 \left[\frac{2 B_V}{B_P} \left(\frac{1 + A^2/B^2}{SNR_A^2} + \frac{2 + 2 A/B}{SNR_A} \right) \right]^{1/2} \text{ dB}$$

where $A \geq B$ (otherwise interchange A and B) and, for the TCP pulse subsystem,

B_V = 7.5 MHz = Video low pass filter bandwidth

B_P = 2 GHz = Pre-D filter bandwidth

A = Amplitude of signal in beam A

The first of the two terms reflects the parabolic (low SNR) detector performance and the second reflects the linear performance region. For the C/D or Σ/Δ measurements, substitute these for A and B in the above formula.

Using the above formula, the measured URSALA antenna patterns, and a 5 dB predetection SNR,

(1) at boresight, Σ = 5 dB and A = B = 2 dB = 1.585

$\sigma_{A/B}$ = 0.69 dB

(2) halfway to the beam edge, A = 4 dB = 2.5, B = 0 dB = 1,

$\sigma_{A/B}$ = 0.75 dB

(3) 3 dB beam edge, A = 6 dB = 4, B = -3 dB = 0.5,

$\sigma_{A/B}$ = 1.12 dB

The above cut was through the center of the A and B beams. P-989 uses 0.88 dB as the average thermal noise monopulse ratio error ($\sigma_{A/B}$) over the beam at 5 dB SNR. The thermal noise error in the TCF pulse collection system is then

$$\sigma_N \text{ (TCFP)} = (0.88)\ (0.06\ B)\ (1/\sqrt{N})\ 10^{(\text{Ref. SNR}-\text{SNR})/20}$$

$$= 0.053\ (B/\sqrt{N})\ 10^{(5-\text{SNR})/20}$$

where N is the number of pulses in the processed intercept. With the 20 dB additional sensitivity of the TCF CW subsystem, this becomes

$$\sigma_N \text{ (TCFCW)} = 0.0053\ (B/\sqrt{N})\ 10^{(5-\text{SNR})/20}$$

where SNR is the SNR in the 2 GHz IF bandwidth and N is now the number of sweeps of the 8 MHz CW filter pair.

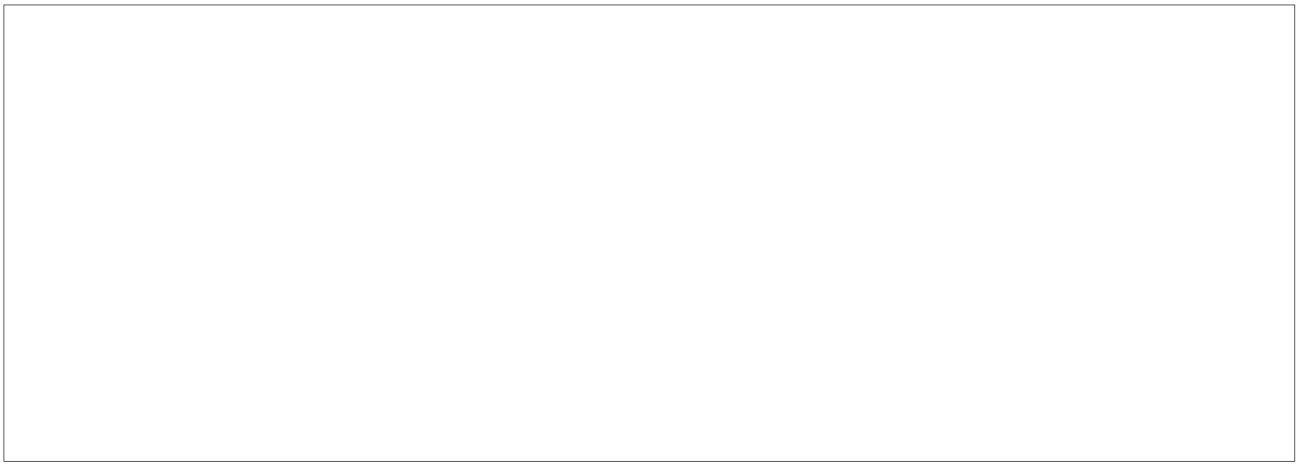

5.2.2 Non-Thermal Noise

In addition to thermal noise, quantization effects, and various mismatches create monopulse errors which are basically independent from pulse-to-pulse but not dependent on the intercept SNR. The monopulse ratio quantization to 1/8 dB, for example, results in an angular error contribution of

$$\sigma_Q = (0.125/\sqrt{12})\ (0.06\ B/\sqrt{NP_D}) = 0.0022\ B/\sqrt{NP_D}$$

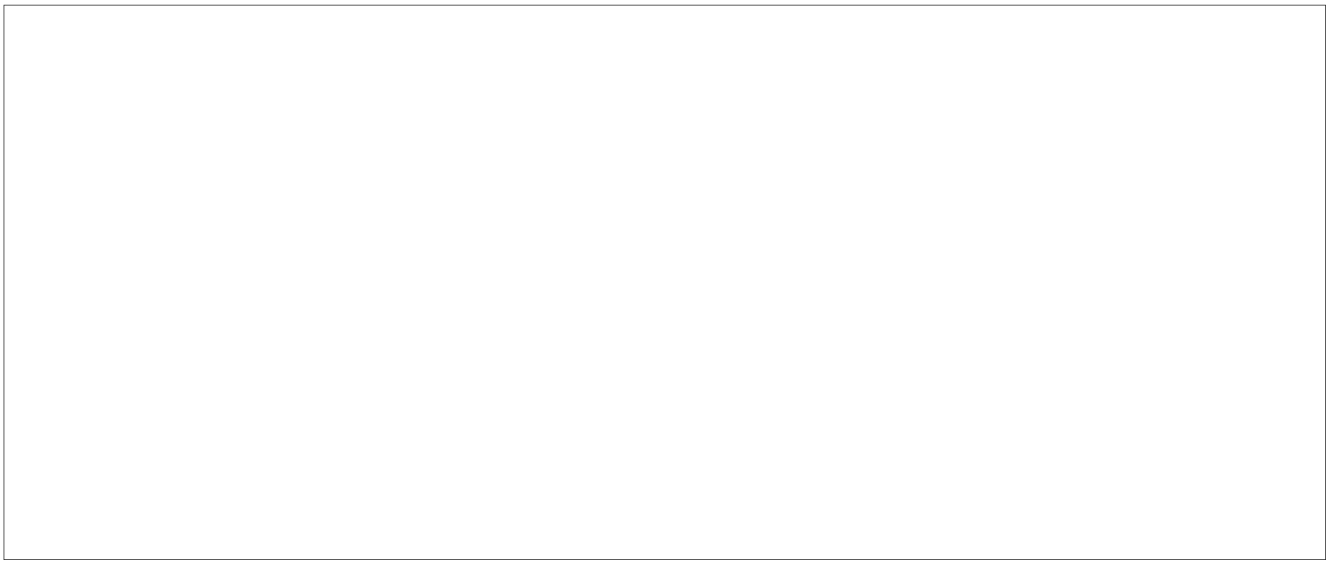

5.3 ERROR BUDGET SUMMARY

The above angular error model is summarized in Table 5-1 and the resultant performance is shown in Fig. 5-1 and 5-2.

Table 5-1
FARRAH ONE-SIGMA GEOLOCATION ERROR BUDGET

SOURCE	ERROR
Ephemeris IT X CT X ALT	[redacted]
Emitter Altitude	
Platform Attitude	
Polarization (Axial Ratio)	
Channel Mismatch	
Thermal Noise	
Quantization (1/8 dB)	
A/D Imperfections	
Model Mismatch	

B = 64 λ/D = antenna 3-dB beamwidth

NP_D = number of pulses (CW sweeps) processed

SNR = dB signal to noise ratio in 2 GHz

C = dB sensitivity improvement of the other implementations relative to the TCF pulse receiver

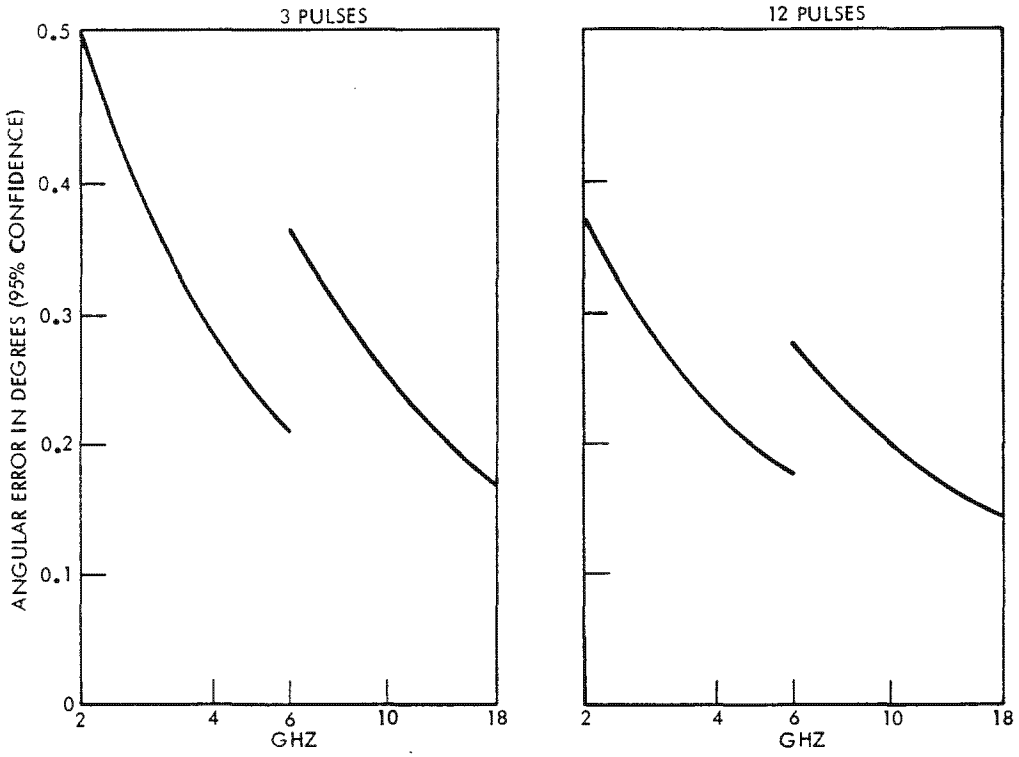

Fig. 5-1 Angular Error Budget at 5 dB SNR

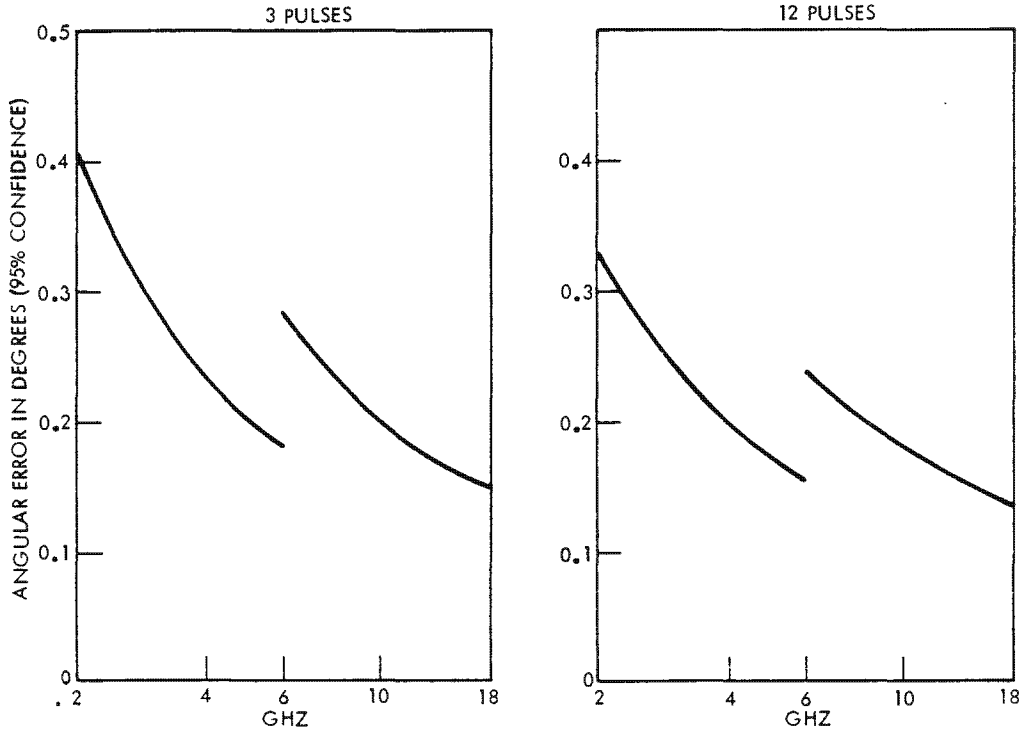

Fig. 5-2 Angular Error Budget at 10 dB SNR